Vibration Frequencies of $Ca_3Fe_2Si_3O_{12}$ Andradite: An ab Initio Study with the CRYSTAL Code

F. Pascale,[†] M. Catti,[‡] A. Damin,[§] R. Orlando,*[,||] V. R. Saunders,[§] and R. Dovesi[§]

Laboratoire de Cristallographie et Modélisation des Matériaux Minéraux et Biologiques, Université Henri Poincaré, BP 239, 54506 Vandœuvre les Nancy Cedex 05, France, Dipartimento di Scienza dei Materiali, Università di Milano Bicocca, via Cozzi 53, 20125 Milano, Italy, Dipartimento di Chimica IFM, Università di Torino, Via P. Giuria 5, 10125 Torino, Italy, and Dipartimento di Scienze e Tecnologie Avanzate, Università del Piemonte Orientale, Via Bellini 25/G, 15100 Alessandria, Italy

Received: June 6, 2005; In Final Form: August 4, 2005

The vibrational spectrum of $Ca_3Fe_2Si_3O_{12}$ andradite is calculated at the Γ point by using the periodic ab initio CRYSTAL program that adopts an all-electron Gaussian-type basis set and the B3LYP Hamiltonian. The full set of frequencies (17 IR active, 25 Raman active, and 55 inactive modes) is calculated. The effect of the basis set on the calculated frequencies is discussed. The modes are characterized by direct inspection of the eigenvectors and isotopic substitution. The present calculations permit us to clarify some of the assignment problems raised by experiments. The mean absolute differences of the various modes with respect to the available experimental IR and Raman data are as small as 9 and 5 cm^{-1}, respectively.

Introduction

Garnets $X^{II}_3Y^{III}_2Si_3O_{12}$ are important rock-forming silicates, as major constituents of the Earth's upper mantle and relevant phases of high-pressure metamorphic rocks in the Earth's crust.[1] Their cubic crystal structure (*Ia*$\bar{3}$*d* space group) is built up by SiO_4 tetrahedra sharing corners with the YO_6 octahedra, whereas the X divalent cations are in dodecahedral coordination. By appropriate chemical substitutions, they give rise to well-known materials for laser technology (e.g., yttrium−aluminum garnets). In the case of andradite (X = Ca, Y = Fe), interesting applications as a material for immobilization of Pu-containing nuclear wastes are under development.[2,3]

The vibrational spectroscopy of several members of the garnet family has been investigated: See the single-crystal IR reflectance studies of Hofmeister et al.[4] and the Raman spectra studies by Hofmeister and Chopelas,[5] Gillet et al.,[6] and Kolesov and Geiger[7,8] (see also ref 9 for experiments before 1990). With regards to theoretical studies, the paper by Chaplin et al.[9] is worth mentioning, where the full set of frequencies of pyrope (magnesium−aluminum garnet) at the Γ point were calculated: There are four formula units (80 atoms) in the primitive cell, generating 240 vibrational modes. Other authors[10−12] computed the elastic constants and the full phonon spectrum of one or more members of the garnet family and explored the effect of pressure and temperature on the structural and dynamical properties or investigated the pyrope−grossular garnet solid solution. All these simulations were based on semiempirical force-field or shell-model-like schemes, the parameters of the models being obtained by best-fitting experimental data of simple oxides (MgO, CaO, Al_2O_3, and SiO_2). Kolesov and Geiger[8] discussed in very clear terms the problems with all of these simulations and concluded that they were unable to simulate the spectra of pyrope correctly. Concerning andradite, both single-crystal IR and Raman experimental results are available;[5,7] also the elastic constants under pressure[13] and the equation of state were measured up to 1000 K and 5 GPa.[14]

It has been shown in a previous paper[15] that the full vibrational spectrum of pyrope garnet can be calculated quantum mechanically with CRYSTAL,[16] an ab initio, periodic, all-electron computer program that uses a Gaussian-type basis set for representing the crystalline orbitals. Our method, which is based on the calculation of the Hessian matrix by numerical differentiation of the analytical energy gradients with respect to the nuclear positions, had already proved to be effective in the calculation of the vibrational spectra of α-quartz. In fact, in previous studies,[17,18] the effect of the computational parameters controlling the accuracy of the calculated vibration frequencies of α-quartz, as well as basis set and Hamiltonian effects, was discussed at length, showing that the B3LYP[19] Hamiltonian provides wavenumbers that are very close to experiment (mean absolute difference within 6−7 cm^{-1}).

In the present paper, we extend our analysis to andradite $Ca_3Fe_2Si_3O_{12}$. Despite a similar structure to pyrope, andradite is much more demanding in terms of computational cost and efficiency of the code. Indeed, the substitutions of the much heavier Ca and Fe atoms for Mg and Al require a substantially larger all-electron basis set. Moreover, because of the $3d^5$ shell configuration of the Fe^{3+} ion, an open-shell treatment is necessary, implying a double diagonalization of the Fock matrix for spin-up and spin-down electrons. The capability of reproducing the spectrum of this system accurately opens the way to simulating the vibrational properties of the whole garnet family, at least for the members containing ions up to the first transition series. Then it will be possible to account for the wavenumber spectrum dependence on the chemical composition in terms of quantum-mechanical properties of chemical bonding in the garnet structure.

* To whom correspondence should be addressed. E-mail: roberto.orlando@unito.it.
[†] Université Henri Poincaré.
[‡] Università di Milano.
[§] Università di Torino.
[||] Univerisità del Piemonte Orientale.

10.1021/jp052991e CCC: $30.25
Published on Web 09/08/2005

TABLE 1: Andradite Structural Properties Calculated with Four Different Basis Sets (BSA-D)

	BSA	BSB	BSC	BSD	exp[a]
N[b]	1560	1608	1640	1740	
ΔE[c]	0.06491	0.03496	0.01443		
a[d]	12.1714	12.1769	12.18930	12.1960	12.051
O_x[e]	0.03882	0.03877	0.038827	0.03893	0.03914
O_y[e]	0.04841	0.04826	0.048338	0.04838	0.04895
O_z[e]	0.65601	0.65590	0.656095	0.65617	0.65534
Ca_1-O[f]	2.3731	2.3739	2.3760	2.3780	2.3584
Ca_2-O[f]	2.5271	2.5296	2.5318	2.5331	2.4953
Fe−O[f]	2.0435	2.0426	2.0473	2.0497	2.0186
Si−O[f]	1.6602	1.6616	1.6615	1.6612	1.6492

[a] Armbruster and Geiger $T = 100$ K (1993); see ref 25. [b] N is the number of basis functions (atomic orbitals) in the primitive cell. [c] ΔE is the energy difference with respect to the total energy evaluated with BSD (−25329.24952 hartree). [d] a is the lattice parameter (Å). [e] O_i are oxygen fractional coordinates. [f] Ca_1-O, Ca_2-O, Fe−O, and Si−O denote interatomic distances (Å).

The structure of the paper is as follows. We first summarize the method employed in the calculation of vibrational spectra and the adopted basis set. The full calculated vibrational spectrum is then presented in the Results, along with an analysis of basis set effects and comparison with experiment.

I. Computational Methods

A developmental version of the CRYSTAL program[16] has been used for the present calculations. In analogy with a previous paper on pyrope,[15] the B3LYP Hamiltonian[19] has been adopted. It contains a hybrid Hartree−Fock/density-functional exchange-correlation term and is widely and successfully used in molecular quantum chemistry[20] as well as in solid-state calculations, where it has been shown to reproduce equilibrium geometry and vibration frequencies[18,21] in excellent agreement with experiment.[18,23] In the present study, the same computational conditions (tolerances for the truncation of the infinite Coulomb and exchange sums, SCF convergence criteria, grid for the integration of the DFT exchange and correlation contribution, and number of reciprocal space points) have been used as for pyrope.[15] For a more extensive analysis of the computational details, we refer to ref 17. To discuss the effect of the variational basis on the calculated geometry and vibrational spectra, four all-electron basis sets of increasing size have been adopted. The simplest one,[24] to be denoted as BSA, contains 8-6511G(3), 8-6411G(41), 8-631G(1), and 8-411G(1) contractions for Ca, Fe, Si, and O, respectively (d function contractions are given in parentheses; 41 means that there are 2d shells at Fe, the first resulting from a 4G contraction, the latter containing a single Gaussian); the exponents (in $bohr^{-2}$ units) of the most diffuse sp and d shells are 0.28(sp) and 0.38(d) (Ca), 0.55 and 0.43 (Fe), 0.29 and 0.6 (Si), and 0.20 and 0.50 (O). This basis set has ionic character, because relatively high exponents are used for the external Gaussians on each cation. A diffuse sp shell is added to Si (0.13) to form basis set B (BSB). One further sp shell is added to Fe (0.25) to form basis set C (BSC). In BSC, functions for allocating diffuse valence electrons are available for both Si and Fe. Finally, BSD is obtained by splitting the 3d contraction for Ca (2d + 1d) and adding a single Gaussian d shell to Fe (0.25). The energy differences with respect to the BSD total energy (per primitive cell) are reported in Table 1 for all basis sets, together with the optimized structural parameters. The importance of the 3d split functions at Ca on the BSD total energy is very small, whereas the addition of a diffuse d shell to the Fe basis set is responsible for most of the energy gain over the BSC result. The difference with respect to experiment is 0.1 Å for the lattice parameter (less than 1%) and 0.01−0.02 Å for the quoted bond distances.

TABLE 2: Calculated (BSD) Vibration Frequencies (cm^{-1}) of Andradite Labeled by Symmetry

F_{1u}	124.0	F_{2u}	240.4	F_{1u}	335.9	F_{2u}	475.7	F_{2g}	806.5
F_{2u}	129.4	F_{2u}	254.9	F_{1g}	343.4	F_{1g}	476.1	F_{1u}	811.7
F_{1u}	146.0	F_{2g}	260.0	B_g	343.8	F_{2g}	490.5	E_g	816.1
F_{2u}	155.8	B_u	260.7	E_g	344.3	E_g	493.3	B_u	828.6
B_u	161.8	F_{1u}	265.2	F_{2g}	350.0	E_u	495.4	F_{1g}	830.2
F_{2g}	163.1	F_{2u}	270.6	F_{2u}	352.1	F_{1u}	499.0	F_{2u}	830.7
F_{1g}	170.0	F_{1g}	270.7	F_{1g}	355.8	A_{1g}	514.9	F_{2g}	834.0
E_g	170.7	E_u	277.5	F_{1u}	362.9	F_{1g}	539.1	E_u	837.5
E_u	174.9	F_{1g}	277.9	F_{2u}	364.5	B_g	544.3	F_{2u}	850.0
F_{1g}	175.8	F_{1u}	279.1	A_{1g}	364.7	F_{2u}	545.8	E_u	853.0
B_g	178.3	E_g	291.8	E_u	365.0	F_{2g}	554.1	A_{1g}	856.3
F_{1u}	181.4	F_{1g}	300.7	E_g	376.2	F_{2u}	563.0	E_g	867.1
F_{2u}	192.8	F_{2g}	303.8	E_u	394.3	E_g	571.0	F_{1u}	867.5
F_{1u}	202.7	F_{2u}	303.8	A_{1u}	415.6	F_{1u}	584.6	F_{1g}	907.5
F_{1g}	214.7	F_{1u}	306.3	B_u	420.9	E_u	587.8	A_{1u}	924.8
E_u	219.7	E_u	311.9	B_g	421.9	F_{2g}	604.2	B_g	962.2
F_{2g}	221.0	F_{2g}	320.7	F_{1u}	426.8	A_{1u}	617.9	F_{2g}	990.0
A_{1u}	222.7	A_{1u}	327.1	F_{1g}	443.6	F_{1u}	793.2		
F_{2g}	228.9	F_{2u}	331.1	F_{2g}	448.0	F_{1g}	793.3		
F_{1u}	238.2	B_u	334.6	F_{1u}	469.7	F_{2u}	798.3		

With regards to the calculation of vibrational spectra, we refer to previous papers[15,17,18] for details and discussion of numerical accuracy. Here we simply recall that, within the harmonic approximation, frequencies at the Γ point have been obtained by diagonalizing the mass-weighted Hessian matrix, W, whose (i,j) element is defined as $W_{ij} = H_{ij}/(M_iM_j)^{1/2}$, where M_i and M_j are the masses of the atoms associated with the i and j coordinates, respectively.

It should be noted that, once the Hessian matrix H is calculated, wavenumber shifts due to isotopic substitutions can readily be calculated simply by changing masses in the above formula. In the present case, isotopic effects have been estimated for the substitution of ^{44}Ca for ^{40}Ca, ^{59}Fe for ^{56}Fe, ^{30}Si for ^{28}Si, and ^{18}O for ^{16}O. First derivatives of energy with respect to the atomic positions, $v_j = \partial V/\partial u_j$, are calculated analytically for all u_j coordinates (u_j is the displacement coordinate with respect to equilibrium), whereas second derivatives at $u = 0$ are calculated numerically using a single displacement

$$\left[\frac{v_j}{u_i}\right]_0 \approx \frac{v_j(0,\cdots,u_i,\cdots)}{u_i}$$

A corrective term should be added to the Hessian in order to obtain the transverse optic−longitudinal optic (TO−LO) splitting for the F_{1u} modes.[15,17] Such a correction, however, has not been considered in the present case, as the implementation of the corresponding part of the program has not yet been completed.

II. Results and Discussion

A. Basis Set Effects and Comparison with Experiment. The highly symmetric garnet structure contains 48 point-symmetry operators and belongs to the O_h point group. The decomposition of the reducible representation built on the basis of the Cartesian coordinates of the atoms in the unit cell leads to the following symmetry assignment for the 240 normal modes (this analysis is performed automatically by the CRYSTAL code)[16]

$$\Gamma_{\text{total}} = 3A_g + 5B_g + 8E_g + 14F_{1g} + 14F_{2g} + 5A_u + 5B_u + 10E_u + 18F_{1u} + 16F_{2u}$$

TABLE 3: Transverse Optical (TO) Infrared-Active Modes (F_{1u}) of Andradite as a Function of the Basis Set Size[a]

	calculated modes								
	BSA		BSB		BSC		BSD		
	ν	$\Delta\nu$	ν	$\Delta\nu$	ν	$\Delta\nu$	ν	$\Delta\nu$	observed modes (ref 5)
	873.7	−1.9	871.6	−4.0	871.2	−4.4	867.5	−8.1	875.6
	817.0	−4.8	815.3	−6.5	815.3	−6.5	811.7	−10.1	821.8
	797.7	2.4	796.1	0.8	796.3	1.0	793.2	−2.1	795.3
	601.4	13.0	592.8	4.4	590.1	1.7	584.6	−3.8	588.4
	509.0	3.7	505.7	0.4	503.8	−1.5	499.0	−6.3	505.3
	477.9	−0.9	476.6	−2.2	474.4	−4.4	469.7	−9.1	478.8
	439.4	6.7	435.6	2.9	433.5	0.8	426.8	−5.9	432.7
	370.6	−3.5	370.2	−3.9	366.2	−7.9	362.9	−11.2	374.1
	345.8	−3.9	346.2	−3.5	341.8	−7.9	335.9	−13.8	349.7
	315.5	−8.2	321.6	−2.1	316.7	−7.0	306.3	−17.4	323.7
	290.3	−14.7	296.3	−8.7	289.4	−15.6	279.1	−25.9	∼305
	274.2	−20.8	277.4	−17.6	271.9	−23.1	265.2	−29.8	295(?)
	246.9	0.3	248.9	2.3	243.1	−3.5	238.2	−8.4	246.6
	209.6	−3.8	210.1	−3.3	206.2	−7.2	202.7	−10.7	213.4
	186.5	−1.1	186.2	−1.4	183.7	−3.9	181.4	−6.2	187.6
	149.7	−2.4	152.4	0.3	147.7	−4.4	146.0	−6.1	152.1
	128.2	−4.6	132.0	−0.8	123.8	−9.0	124.0	−8.8	132.8
$\lvert\bar{\Delta}\rvert$		+4.1 (+5.7)		+2.6 (+3.8)		+4.7 (+6.5)		+8.5 (+10.8)	
$\bar{\Delta}$		−0.6 (−2.6)		−1.1 (−2.5)		−4.3 (−6.0)		−8.5 (−10.8)	
Δ_{min}		(−8.2) (−20.8)		−6.5 (−17.6)		−9.0 (−23.1)		−17.4 (−29.8)	
Δ_{max}		+13.0 (+13.0)		+4.4 (+4.4)		+1.7 (+1.7)		0.0 (0.0)	

[a] Frequency differences ($\Delta\nu$) and statistical indices (see text for definitions) evaluated with respect to the experimental data reported in the last column, where modes at 295 and 305 cm^{-1} have been excluded. Data in parentheses refer to the full set.

Seventeen F_{1u} modes are IR active (one F_{1u} mode corresponds to translations); twenty-five modes are Raman active ($3A_{1g} + 8E_g + 14F_{2g}$). Fifty-five modes are inactive.

The full set of 97 frequencies calculated with BSD is reported in Table 2, along with symmetry classification. The spectrum can be divided into two parts: the high wavenumber part, from 793 to 990 cm^{-1}, contains the 48 symmetric and antisymmetric Si−O stretching modes and is separated by a large gap of about 170 cm^{-1} from the rest of the spectrum that contains all the other modes in a continuum ranging from 124 to 617 cm^{-1}.

In this section we will mainly focus on the IR and Raman active modes where comparison with experiment is possible. Experimental (ν_υ^{exp}) and computed (ν_υ) vibration frequencies are compared both analytically and through the following four global indices

$$|\bar{\Delta}| = \frac{1}{N}\sum_{\upsilon=1}^{N} |\nu_\upsilon - \nu_\upsilon^{exp}|$$

$$\bar{\Delta} = \frac{1}{N}\sum_{\upsilon=1}^{N} \nu_\upsilon - \nu_\upsilon^{exp}$$

$$\Delta_{max} = \max(\nu_\upsilon - \nu_\upsilon^{exp})$$

$$\Delta_{min} = \min(\nu_\upsilon - \nu_\upsilon^{exp})$$

$$\upsilon = 1, 2, ...$$

In Table 3 the experimental IR frequencies obtained by Hofmeister and Chopelas[5] are reported, together with the calculated frequencies obtained with the four basis sets of increasing size (BSA, BSB, BSC, and BSD) described in the previous section. Hofmeister and Chopelas[5] report a full set of 17 IR frequencies; however, two of them are affected by a relatively large uncertainty: In their Table 3, the authors indicate one mode at "∼305" cm^{-1}, whereas a second mode at 295 cm^{-1} is labeled as "position uncertain".[5]

The effect of the basis set on the determination of equilibrium geometry and total energy is shown in Table 1. Geometry modifications in going from BSA to BSD are extremely small, despite basis set improvement. On the other hand, the influence of the basis set on the calculated frequencies is larger, as shown in Table 3, the main variation being due to one additional d function of Fe (and splitting of the d shell of Ca) when going from BSC to BSD. The variability of individual frequencies, however, is in the range of 17 cm^{-1}, and in most cases it is smaller than 10 cm^{-1}. In all cases the mean absolute difference with respect to experiment, $|\bar{\Delta}|$, is very small (it is 4.1, 2.6, 4.7, and 8.5 cm^{-1} when going from BSA to BSD, see Table 3, similar to the values we obtained for pyrope).[15]

It is worth noting that the largest (our "best") basis set used gives results with the largest value of $|\bar{\Delta}|$. This can be explained by considering that, with an incomplete basis set, two sources of error exist, namely, the approximate Hamiltonian and the basis set finiteness, which tend to cancel in the present case. When one of these error sources becomes negligible, as in the case of a nearly complete basis set like BSD, this cancellation cannot occur. Therefore, BSB appears to perform better, with $|\bar{\Delta}|$ values as small as 2.6 cm^{-1}. At the BSD level, all the calculated frequencies are smaller than the experimental values. This is a consequence of the overestimation of the lattice parameter (see Table 1), a typical effect of the B3LYP Hamiltonian when heavy atoms such as Ca and Fe are involved: larger equilibrium distances imply softer modes. In the case of pyrope,[15] where lighter atoms are involved (Mg and Al instead of Ca and Fe), the lattice parameter overestimation is smaller (0.10 instead of 0.14 Å) and the frequencies are not so systematically underestimated with respect to experiment (compare the mean value of the differences, $\bar{\Delta}$, decreasing from +10 to −2 cm^{-1} with the decrease in $\bar{\Delta}$ for andradite from −0.6 to −8.5 cm^{-1}).

The agreement between the BSD calculated frequencies and experiment is generally very good, with differences below 20 cm^{-1} for all but two modes, respectively, at 265.2 (exp, 295) and 279.1 (exp, 305) cm^{-1}. Both of these modes have been mentioned above for a relatively large uncertainty in their experimental determination. Thus, we may conclude that a good agreement with experiment is achieved for the IR modes.

TABLE 4: Calculated and Experimental Raman Vibration Frequencies of Andradite (cm^{-1})

	calculated modes								observed modes	
	BSA		BSB		BSC		BSD			
	ν	$\Delta\nu$[a]	ν	$\Delta\nu$	ν	$\Delta\nu$	ν	$\Delta\nu$	ref 7	ref 5
F_{2g}	1004.4	9.4	996.4	1.4	993.4	−1.6	990.0	−5.0	995	995
E_g	872.1	−1.9	870.0	−4.0	869.5	−4.5	867.1	−6.9	874	874
A_{1g}	871.1	(−0.9)[b]	861.1	(−10.9)	857.0	(−15.0)	856.3	(−15.7)	-	872
F_{2g}	838.6	−3.4	836.2	−5.8	836.4	−5.6	834.0	−8.0	842	842
E_g	824.3	(−18.7)	818.3	(−24.7)	818.8	(−24.2)	816.1	(−26.9)	-	843
F_{2g}	810.8	−5.2	809.6	−6.4	808.9	−7.1	806.5	−9.5	816	816
F_{2g}	623.1	(30.1)	613.1	(20.1)	609.1	(16.1)	604.2	(11.2)	-	593
E_g	582.9	8.9	576.5	2.5	574.9	0.9	571.0	−3.0	574	576
F_{2g}	573.8	20.8	560.1	7.1	558.8	5.8	554.1	1.1	553	553
A_{1g}	526.6	10.6	521.4	5.4	518.9	2.9	514.9	−1.1	516	516
E_g	505.9	13.9	500.2	8.2	498.9	6.9	493.3	1.3	492	494
F_{2g}	498.1	4.1	494.9	0.9	493.8	−0.2	490.5	−3.5	494	494
F_{2g}	461.0	9.0	456.8	4.8	454.1	2.1	448.0	−4.0	452	452
E_g	383.5	1.5	382.6	0.6	380.7	−1.3	376.2	−5.8	382	370
A_{1g}	375.2	5.2	387.3	17.3	373.2	3.2	364.7	−5.3	370	370
F_{2g}	358.2	(−23.8)	356.5	(−25.5)	355.6	(−26.4)	350.0	(−32.0)		382
E_g	349.9	−2.1	349.5	−2.5	347.9	−4.1	344.3	−7.7	352	352
F_{2g}	328.9	3.9	328.4	3.4	325.2	0.2	320.7	−4.3	325	325
F_{2g}	309.6	−2.4	310.8	−1.2	309.3	−2.7	303.8	−8.2	312	311
E_g	299.7	1.7	300.1	2.1	299.2	1.2	291.8	−6.2	298	296
F_{2g}	265.9	1.9	264.6	0.6	263.7	−0.3	260.0	−4.0	264	264
F_{2g}	233.6	−2.4	232.3	−3.7	232.0	−4.0	228.9	−7.1	236	235
F_{2g}	226.3	(−2.7)	225.1	(−3.9)	224.6	(−4.4)	221.0	(−8.0)		229
E_g	174.9	0.9	173.9	−0.1	172.8	−1.2	170.7	−3.3	174	173
F_{2g}	169.6	−4.4	167.7	−6.3	165.7	−8.3	163.1	−10.9	174	173
$\|\bar{\Delta}\|$		5.7 (7.9)		4.2 (7.1)		3.2 (6.2)		5.3 (7.8)		
$\bar{\Delta}$		3.5(2.7)		1.2 (−0.3)		−0.9 (−2.3)		−5.1 (−6.4)		
Δ_{min}		−5.2 (−23.8)		−6.4 (−25.5)		−8.3 (−26.4)		−10.9 (−32.0)		
Δ_{max}		20.8 (30.1)		17.3 (20.1)		6.9 (16.1)		1.3 (11.2)		

[a] $\Delta\nu$ measures the difference with respect to data in ref 7 that are used in the calculation of the statistical indices at the bottom of the table (see text for definitions). [b] Data in parentheses refer to ref 5.

Hofmeister and Chopelas[5] also report a full set of 25 Raman modes, one of which at 872 cm^{-1} is quoted as "slightly uncertain" (last column in Table 4). More recently (1998), Kolesov and Geiger[7] reported a subset of 20 of these modes (see Table 4), which differ from the previous experimental data by less than 1 cm^{-1}. The remaining five modes, that are only reported by Hofmeister and Chopelas, are, indeed, those with the worst disagreement with the values calculated with BSD (872, 843, 593, 382, and 229 cm^{-1}): $\nu_v - \nu_v^{exp}$ is −15.7, −26.9, −11.2, −32.0, and −8.0 cm^{-1}, respectively, whereas the largest deviation of the other 20 modes is −10.9 and it corresponds to the lowest frequency mode. Kolesov and Geiger did not report these five modes, and this suggests that the mode at 872 cm^{-1} is probably not the only one determined with a large uncertainty. For this reason, the terms reported in Table 4 refer to the subset of 20 vibrational frequencies, and the comparison to the full set is reported in parentheses. Again, the best basis set (BSD) does not provide the best agreement of simulated Raman frequencies with experiment. However, the mean absolute error $|\bar{\Delta}|$ is small, even smaller than that for IR, that is, 5.3 and 8.5 cm^{-1}, respectively.

We conclude that the calculated Raman vibration frequencies reproduce the experimental spectrum accurately.

B. Analysis of the Spectrum and Comparison with Pyrope. In our paper on pyrope,[15] the problem of vibrational mode classification for garnets in terms of simple categories such as symmetric and antisymmetric stretching (ν_1 and ν_3) or bending (ν_2 and ν_4) of the SiO_4 units, their rotations $R(SiO_4)$ and translations $T(SiO_4)$ or T(Mg) and T(Al) was discussed at length. Such a description appears to be suitable for those systems consisting of fully covalent or fully ionic moieties, like, for example, in $CaCO_3$,[21] where the gap between inner and translation−rotation modes is larger than 300 cm^{-1}, despite strong coupling of translations and rotations of the group CO_3 with translations of the Ca cation (see final section in ref 21).

In garnets a similar classification in terms of group (SiO_4) and "free cations" (Fe and Ca, in this case) is difficult. Kolesov and Geiger[7] were the first to show experimentally that mode coupling is present in the Raman spectra of garnet. The aspect of coupling was further emphasized in ref 22. Therefore, direct inspection of the modes by means of graphical representation, as we did in our study of pyrope where we showed animations of the IR and Raman modes, can be more effective.

The vibrational modes of andradite are in many aspects similar to pyrope, and a one-to-one correspondence can be established in most cases. For this reason, the main features of the andradite spectrum will be illustrated and discussed with quantitative comparison to pyrope in Tables 5 and 6 and Figures 1−4, where the effect of various isotopic substitutions is shown.

The figures show very clearly that the vibrational spectrum can be divided into two parts: the upper part containing the 48 stretching modes (ν_1 and ν_3) and the lower part including the remaining modes and forming a continuum in the range from 124 to 617 cm^{-1}. The large gap (170 cm^{-1}) between the two correponds to the substantial independence of Si−O stretching modes from other modes, as is documented by the negligible involvement of Ca and Fe (see Figures 2 and 3 and Tables 5 and 6). The classification of stretching modes by symmetry can be obtained directly by reducing the representation obtained from the 48 Si−O basis vectors

$$\Gamma_{Si-O} = A_g + B_g + 2E_g + 3F_{1g} + 3F_{2g} + A_u + B_u + 2E_u + 3F_{1u} + 3F_{2u}$$

TABLE 5: Effect of the ^{44}Ca, ^{59}Fe, ^{30}Si, and ^{18}O Isotopic Substitution on the Calculated IR-Active (TO) Modes (F_{1u} Symmetry) of Andradite[a]

$Ca_3Fe_2Si_3O_{12}$ ν^b	^{44}Ca (^{26}Mg) $\Delta\nu^b$	^{59}Fe (^{29}Al) $\Delta\nu$	^{30}Si $\Delta\nu$	^{18}O $\Delta\nu$
867.5 (969.7)	−0.1 (−0.3)	−0.1 (0.0)	−12.9 (−12.4)	−26.2(−31.9)
811.7 (895.9)	0.0 (−0.1)	−0.1 (0.0)	−11.4 (−11.2)	−26.1(−30.9)
793.2 (864.8)	−0.1 (−0.1)	−0.1 (−0.1)	−11.7 (−11.5)	−24.6(−28.9)
584.6 (674.1)	−0.3 (−1.1)	−0.4 (−3.5)	−4.2 (−4.4)	−26.0 (−24.3)
499.0 (582.9)	−0.4 (−0.5)	−0.7 (−7.4)	−4.0 (−2.7)	−20.4 (−15.6)
469.7 (532.8)	−0.3 (−0.1)	−0.4 (−5.8)	−4.1 (−3.8)	−19.4 (−13.1)
426.8 (483.6)	0.0 (−0.5)	−0.1 (−1.3)	−0.3 (−1.1)	−23.9 (−21.9)
362.9 (459.0)	−7.7 (−0.3)	−0.6 (−9.9)	−0.7 (−0.4)	−8.6 (−11.1)
335.9 (423.0)	−0.9 (−0.2)	−0.1 (−6.8)	−0.6 (−2.4)	−17.5 (−9.1)
306.3 (382.9)	−1.1 (−0.2)	−1.3 (−4.3)	−0.1 (−1.0)	−12.3 (−13.7)
279.1 (348.6)	−0.3 (−0.1)	−3.8 (−1.7)	−0.9 (−1.6)	−6.3 (−14.1)
265.2 (334.2)	−1.9 (−5.3)	−3.1 (−0.8)	−0.7 (−1.3)	−6.1 (−8.4)
238.2 (259.9)	−2.4 (−3.4)	−2.6 (−0.4)	−1.1 (−1.8)	−3.1 (−6.9)
202.7 (215.8)	−4.6 (−2.0)	−0.9 (−0.9)	−1.0 (−0.3)	−2.5 (−7.9)
181.4 (189.3)	−4.7 (−5.7)	−0.4 (−0.1)	−0.8 (−0.5)	−3.0 (−1.4)
146.0 (139.8)	−1.1 (−0.8)	−1.5 (−0.5)	−0.7 (−0.9)	−3.0 (−4.8)
124.0 (121.1)	−3.2 (−3.7)	−1.1 (−0.4)	−0.1 (−0.1)	−0.8 (−0.9)

[a] The corresponding data obtained for pyrope are reported in parentheses (in this case ^{22}Mg and ^{29}Al replace ^{24}Mg and ^{27}Al). [b] ν and $\Delta\nu$ in cm^{-1}.

TABLE 6: Effect of the ^{44}Ca, ^{30}Si, and ^{18}O Isotopic Substitution on the Calculated Raman Modes (A_g, E_g, and F_{2g} Symmetry)[a]

	$Ca_3Fe_2Si_3O_{12}$ ν^b	^{44}Ca (^{26}Mg) $\Delta\nu^b$	^{30}Si $\Delta\nu$	^{18}O $\Delta\nu$
F_{2g}	990.0 (1067.2)	−0.3 (−0.5)	−13.6 (−13.2)	−32.0 (−36.5)
E_g	867.1 (936.3)	−0.2 (−0.2)	−13.8 (−14.3)	−24.6 (−27.3)
A_{1g}	856.3 (923.8)	0.0 (0.0)	0.0 (0.0)	−49.0 (−52.9)
F_{2g}	834.0 (895.9)	0.0 (−0.1)	−12.5 (−12.3)	−25.3 (−28.9)
E_g	816.1 (863.2)	0.0 (0.0)	−0.1 (0.0)	−46.7 (−49.3)
F_{2g}	806.5 (860.6)	0.0 (−0.1)	−12.0 (−12.2)	−24.6 (−27.4)
F_{2g}	604.2 (655.2)	−0.2 (−0.1)	−3.9 (−4.3)	−28.4 (−30.3)
E_g	571.0 (635.8)	−0.4 (−1.2)	−4.6 (−4.9)	−25.2 (−27.4)
F_{2g}	554.1 (607.2)	−0.1 (−0.1)	−1.8 (−1.7)	−28.8 (−31.7)
A_{1g}	514.9 (567.5)	0.0 (0.0)	0.0 (0.0)	−29.5 (−32.5)
E_g	493.3 (530.7)	−0.1 (−0.1)	−0.1 (−0.3)	−28.0 (−30.0)
F_{2g}	490.5 (514.1)	−0.1 (−0.2)	−4.2 (−3.9)	−21.3 (−22.1)
F_{2g}	448.0 (495.3)	−0.1 (−0.2)	−0.8 (−2.5)	−24.2 (−25.2)
E_g	376.2 (378.9) II[c]	−3.0 (−1.9)	−0.2 (−0.4)	−15.4 (−17.3)
A_{1g}	364.7 (356.5) III	0.0 (0.0)	0.0 (0.0)	−20.8 (−20.4)
F_{2g}	350.0 (383.8) I	−0.8 (−0.2)	−0.1 (−3.3)	−18.7 (−15.7)
E_g	344.3 (336.7) II	−5.9 (−4.8)	−0.7 (−0.2)	−13.3 (−12.3)
F_{2g}	320.7 (353.3) I	−0.3 (−0.4)	−4.7 (−2.7)	−10.6 (−16.2)
F_{2g}	303.8 (320.0)	−0.7 (−0.3)	−1.1 (−3.9)	−14.3 (−11.8)
E_g	291.8 (309.3)	−0.2 (−0.2)	0.0 (−0.1)	−16.6 (−17.3)
F_{2g}	260.0 (268.3)	−4.7 (−8.5)	−1.8 (−0.1)	−4.9 (−3.0)
F_{2g}	228.9 (204.2) II	−4.6 (−1.8)	−0.7 (−0.9)	−7.8 (−7.7)
F_{2g}	221.0 (171.9) III	−1.7 (−0.5)	−1.8 (−1.2)	−8.0 (−7.7)
E_g	170.7 (209.2) I	−3.5 (−3.7)	−1.2 (−1.8)	−3.8 (−4.4)
F_{2g}	163.1 (106.5)	−6.6 (−3.4)	−0.3 (−0.1)	−0.9 (−1.3)

[a] No isotopic shift is observable for modes involving Fe as a consequence of being at a centrosymmetric site. The corresponding data for pyrope are reported in parentheses (in this case ^{26}Mg replaces ^{24}Mg). [b] Frequencies (ν) and isotopic shifts ($\Delta\nu$) in cm^{-1}. [c] Roman numerals on the right in the ν column indicate how the frequency order in pyrope has been altered to match the symmetry sequence in andradite.

The corresponding band in pyrope lies at higher wavenumbers (it is 220 cm^{-1} wide in pyrope and 200 cm^{-1} in andradite), but the gap is exactly the same, with the exception of an isolated A_u mode with large participation of Al that appears in the gap of pyrope. This stretching band is red shifted in pyrope with respect to andradite by about 80 cm^{-1}.

A similar shift is observed for most of the modes in the lower band (see Tables 5 and 6 about IR and Raman active modes of pyrope and andradite and their isotopic shift) resulting from

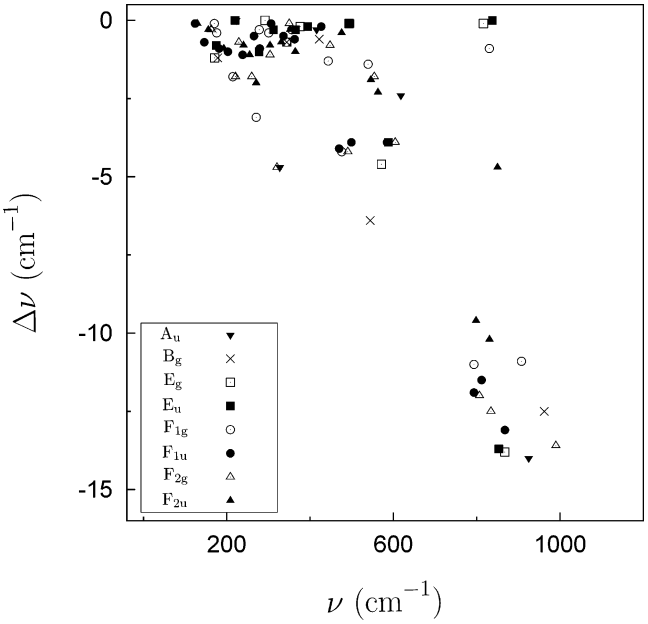

Figure 1. Vibration frequency shifts ($\Delta\nu$) of andradite when ^{30}Si replaces ^{28}Si.

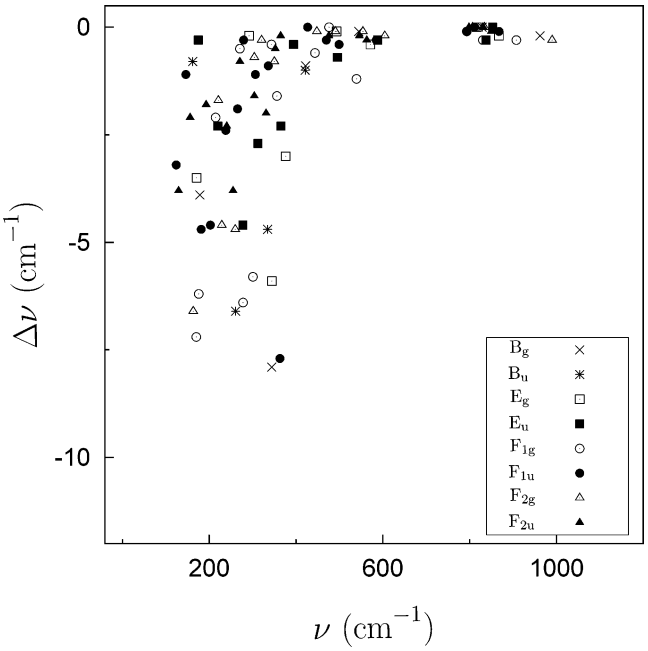

Figure 2. Vibration frequency shifts ($\Delta\nu$) of andradite when ^{44}Ca replaces ^{40}Ca.

the smaller equilibrium volume of pyrope than andradite and a consequent larger "compression" of the SiO_4 tetrahedron. As expected, the main difference is related to the mass of the cations (Ca and Fe, instead of Mg and Al). The vibrational spectrum can be divided into parts where the participation of one of the ions (M) to the modes is mostly important according to the isotopic shift. In the following we will refer to each of these parts as the M-range of wavenumbers. The Mg-range lies between 100 and 300 cm^{-1} in the pyrope spectrum, and the Al-range is between 300 and 618 cm^{-1} (see figures in ref 15). In andradite, the Ca-range is between 124 and 380 cm^{-1} (see Figure 2 and Tables 5 and 6), and the Fe-range lies between 124 and about 350 cm^{-1} (see Figure 3). This means that the part of the andradite spectrum between 618 cm^{-1} (the upper limit of the lower band) and about 400 cm^{-1} includes bending modes of the SiO_4 tetrahedra that are only weakly coupled to

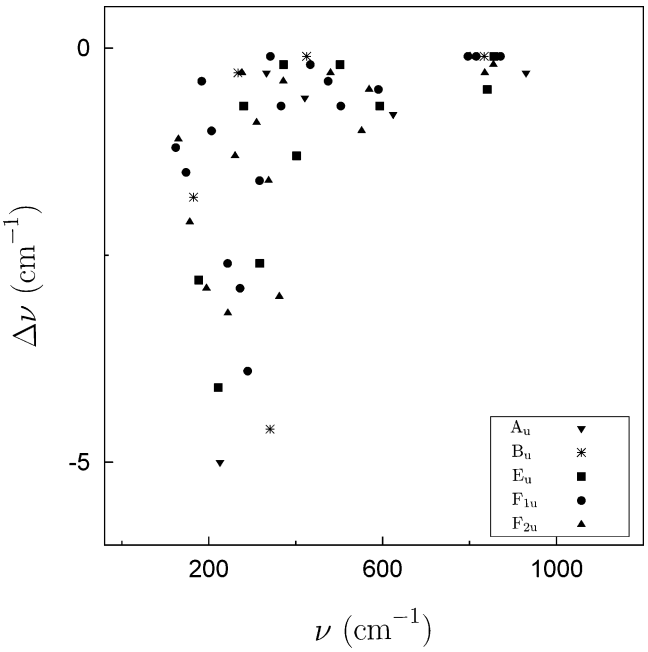

Figure 3. Vibration frequency shifts ($\Delta\nu$) of andradite when ^{59}Fe replaces ^{56}Fe.

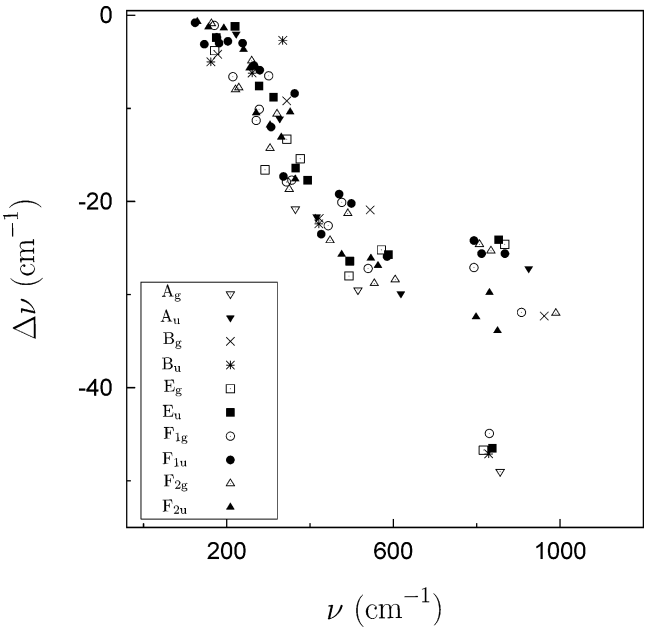

Figure 4. Vibration frequency shifts ($\Delta\nu$) of andradite when ^{18}O replaces ^{16}O.

cation (Ca and Fe) vibrations. This is confirmed by the higher contribution of O and Si in andradite to modes beyond 400 cm^{-1} than in pyrope (see Tables 5 and 6). Only a few symmetry inversions take place in the low-wavenumber portion of the spectrum. The Raman active modes undergoing symmetry inversion are labeled with roman numerals in the second column of Table 6.

Two final comments concerning the comparison of pyrope and andradite spectra can be added:

(a) The Ca-range in andradite extends to higher wavenumbers than the Mg-range in pyrope, despite a large difference in mass acting in the opposite direction; this means that the potential energy surface at the dodecahedra site is much steeper for Ca than for Mg (or that Ca fits the site size, whereas Mg is smaller than the cavity).

(b) Pyrope modes are always higher than the corresponding modes in andradite in the entire 200−1000 cm^{-1} region. Conversely, pyrope modes are below 200 cm^{-1} (see Table 5), so confirming point (a) above: The potential energy surface in the dodecahedral site is softer for Mg than for Ca, as a consequence of the larger size of the latter cation (see refs 7 and 8 for more details and explanations).

III. Conclusions

The present paper shows that it is possible to perform the calculation of the full vibrational spectrum of a large unit cell system containing heavy atoms, such as Fe and Ca, with an open-shell configuration (Fe), by using ab initio quantum mechanical methods and all-electron basis sets. It confirms our previous findings for pyrope,[15] that vibrational frequencies in very good agreement with experiment can be computed for garnets with a large basis set and B3LYP Hamiltonian (mean absolute differences of 6−8 cm^{-1}). In those cases where experimental data are affected by a large uncertainty, a quite accurate positioning of the mode becomes possible.

References and Notes

(1) Deer, W.; Howie, R.; Zussman, J. *An introduction to the rock-forming minerals*; John Wiley: New York, 1992.

(2) Matyunin, Y. I.; Alexeev, O.; Ananina, T. *J. Nucl. Sci. Technol.* **2002**, *Suppl. 3*, 649−651.

(3) Utsunomiya, S.; Yudintsev, S.; Ewing, R. *J. Nucl. Mater.* **2005**, *336*, 251−260.

(4) Hofmeister, A.; Fagan, T.; Campbell, K.; Schaal, R. *Am. Mineral.* **1996**, *81*, 418−428.

(5) Hofmeister, A.; Chopelas, A. *Phys. Chem. Miner.* **1991**, *17*, 503−526.

(6) Gillet, P.; Fiquet, G.; Malézieux, J.; Geiger, C. A. *Eur. J. Mineral.* **1992**, *4*, 651−664.

(7) Kolesov, B. A.; Geiger, C. A. *Phys. Chem. Miner.* **1998**, *25*, 142−151.

(8) Kolesov, B. A.; Geiger, C. A. *Phys. Chem. Miner.* **2000**, *27*, 645−649.

(9) Chaplin, T.; Price, G.; Ross, N. *Am. Mineral.* **1998**, *83*, 841−847.

(10) Mittal, R.; Chaplot, S.; Choudhury, N. *Phys. Rev. B* **2001**, *64*, 094302.

(11) Pavese, A. *Phys. Chem. Miner.* **1999**, *26*, 649−657.

(12) Bosenick, A.; Dove, M. T.; Geiger, C. A. *Phys. Chem. Miner.* **1999**, *26*, 649−657.

(13) Jiang, F.; Speziale, S.; Shieh, S.; Duffy, T. *J. Phys.: Condens. Matter* **2004**, *16*, S1041−S1052.

(14) Pavese, A.; Diella, V.; Pischedda, V.; Merli, M.; Bocchio, R.; Mezouar, M. *Phys. Chem. Miner.* **2001**, *28*, 242−248.

(15) Pascale, F.; Zicovich-Wilson, C. M.; Orlando, R.; Roetti, C.; Ugliengo, P.; Dovesi, R. *J. Phys. Chem. B* **2005**, *109*, 6146−6152.

(16) Saunders, V. R.; Dovesi, R.; Roetti, C.; Orlando, R.; Zicovich-Wilson, C. M.; Harrison, N. M.; Doll, K.; Civalleri, B.; Bush, I. J.; D′Arco, P.; Llunell, M. *Crystal03 user's manual.*; Università di Torino: Torino, Italy, 2003.

(17) Pascale, F.; Zicovich-Wilson, C. M.; Gejo, F. L.; Civalleri, B.; Orlando, R.; Dovesi, R. *J. Comput. Chem.* **2004**, *25*, 888−897.

(18) Zicovich-Wilson, C. M.; Pascale, F.; Roetti, C.; Saunders, V. R.; Orlando, R.; Dovesi, R. *J. Comput. Chem.* **2004**, *25*, 1873−1881.

(19) Becke, A. D. *J. Chem. Phys.* **1993**, *98*, 5648−5652.

(20) Koch, W.; Holthausen, M. C. *A Chemist's Guide to Density Functional Theory*; Wiley-VCH Verlag GmbH: Weinheim, Germany, 2000.

(21) Prencipe, M.; Pascale, F.; Zicovich-Wilson, C.; Saunders, V. R.; Orlando, R.; Dovesi, R. *Phys. Chem. Miner.* **2004**, *31*, 559−564.

(22) Geiger, C. A.; Kolesov, B. A. *European Notes in Mineralogy—Energy Modelling in Minerals*; Eötvös University Press: Budapest, Hungary, 2002; Vol. 4, Chapter 12.

(23) Tosoni, S.; Pascale, F.; Ugliengo, P.; Orlando, R.; Saunders, V. R.; Dovesi, R. *Mol. Phys.* **2005**, in press.

(24) Crystal basis set database. www.chimifm.unito.it/CRYSTAL/basis.html.

(25) Armbruster, T.; Geiger, C. A. *Eur. J. Mineral.* **1993**, *5*, 59−71.